ISSN: 2472-3703 DOI: 10.6911/WSRJ.202504_11(4).0005

Dynamic Response of Surrounding Rock and Supporting Structure of Deep Underground Cavern in Non-water-rich Strata Under Explosion Load

Yongchao Tian[1], Kaifang Ren[1], Haikun Shan[1], Jiaqi Guo[1], Feiyue Sun[2], Xin Huang[1], Yujie Wang[1]

[1]School of Civil Engineering, Henan Polytechnic University, Jiaozuo 454003, China

[2]School of Emergency Management, Henan Polytechnic University, Jiaozuo 454003, China

Abstract

The paper investigates the dynamic response characteristics of deep underground caverns and their supporting structures under explosive loading through numerical simulation. By systematically analyzing the displacement, stress, velocity, acceleration, strain, and plastic zones of underground caverns under different explosive conditions, the following conclusions are drawn: As the peak of explosive pressure increases, the peak velocity significantly increases, and the displacement of the crown settlement and floor heave also increases accordingly. Under explosive loading, the surrounding confinement pressure of the cavern exhibits significant compression and tensile damage, especially in the support area at the bottom of the cavern, which is more sensitive to failure. Therefore, additional reinforcement is required during the design phase. The explosive stress wave induces a dual plastic state in the cavern, including tensile and shear plasticity. As the stress wave propagates, the tensile plastic zone gradually expands, with the expansion rate slowing down over time. The medium elements near the blast hole mainly exhibit tensile-shear failure, while those further away from the blast hole predominantly experience tensile failure. This study provides an important basis for optimizing protective measures in deep underground engineering, particularly in the design of cavern supports and structural reinforcement.

Keywords

Blast load; Non-water-rich strata; Dynamic response; Numerical simulation.

1. INTRODUCTION

With the rapid development of cutting-edge technologies, various types of weapons have made significant breakthroughs in terms of penetration, explosive power, and accuracy. The protection of underground facilities has become an important component of national security. Against this backdrop, strengthening the safety protection measures of underground projects, particularly enhancing the blast resistance of deep underground chambers, holds significant strategic importance.

The response characteristics of underground engineering structures under explosive loading are very complex, and scholars both domestically and internationally have conducted in-depth research in this field. Wang Guangyong et al. [1] used numerical analysis methods to study the vibration velocity distribution patterns of anchored chambers and explored the influence of bolt spacing and length on vibration velocity. Xu et al. [2] conducted field experiments to study the dynamic response characteristics of deep rock masses under blasting loads, comparing the differences between deep and shallow rock masses in resisting explosive loads. Wu et al. [3]

ISSN: 2472-3703 DOI: 10.6911/WSRJ.202504_11(4).0005

employed numerical analysis techniques to evaluate the damage range of surrounding granite during an accidental explosion in an underground ammunition depot, and derived practical formulas for the damage range around the explosion area, the safe burial depth of storage rooms, and the safe distance between adjacent rooms. Wang Guangyong et al. [4], based on blast-resistant model test results, used numerical analysis methods to study the blast resistance of underground chambers under different explosion directions. The research showed that the anchoring effect of bolts leads to a tensile "splitting" phenomenon between bolts, resulting in "layered cracking" phenomena in the anchorage area and its ends. Xu Gancheng et al. [5] proposed a method for reinforcing the surrounding rock of underground chambers with cross-anchor reinforcement and analyzed the blast resistance performance of this method through experimental studies and numerical simulations. Chen Anmin et al. [6] studied the stress and deformation characteristics of the chamber's surrounding rock and lining structure under explosive loading through blast-resistant structural model tests. Deng et al. [7] explored the failure characteristics of jointed circular tunnels under explosive loading, finding that the reinforcing effect of bolts significantly enhanced the tunnel's blast resistance. Through similar physical model tests, some scholars [8,9] examined the effects of different explosive configurations and anchoring methods on the blast resistance of underground chambers, providing important theoretical support for improving the safety of underground structures. Xu Jingmao et al. [10] conducted a series of comparative model tests using Froude similarity theory to study the blast resistance of underground chambers reinforced with locally lengthened or uniformly lengthened bolts at arch feet, analyzing the deformation, failure, and strength characteristics of chambers under different reinforcement methods. The CHANG team [11], using precise numerical simulation techniques, conducted an in-depth analysis of the damage to cement mortar chambers reinforced with aluminum rods under explosive loading, summarizing the damage patterns in rebar areas, non-rebar areas, and combined composite damage modes. Saikat et al. [12] used the three-dimensional discrete element method (3DEC) to carefully analyze the displacement of cave chambers, aiming to deepen the understanding of the behavior of large underground spaces under explosive effects. Amichian [13] used the finite element method to study the spalling characteristics of tunnel surrounding rock under explosive loading, providing an important theoretical basis for tunnel support design. Koneshwaran [14] studied the damage conditions of tunnels under different soil types, explosive amounts, and blast distances, revealing the influence of these factors on tunnel structural safety. Mobaraki [15] researched the dynamic response characteristics of tunnels with different cross-sectional shapes and analyzed the impact of shape factors on tunnel blast resistance.

Currently, the study of the response characteristics of underground chambers under explosive loading mainly relies on three methods: theoretical analysis, experimental research, and numerical simulation. Numerical simulation can visually display the propagation and failure process of stress waves in surrounding rock after an explosion, which helps in monitoring the dynamic response at specific locations. This paper uses three-dimensional finite difference software to analyze key indicators such as displacement, stress, velocity, acceleration, strain, and plastic zones of underground chambers under different explosive conditions, aiming to reveal the dynamic response characteristics of deep underground chambers and their supporting structures under explosive loads.

2. NUMERICAL MODEL BUILDING PROCESS

2.1. Model Building

The model is set with a horizontal direction (X-axis) of 50 m, a vertical direction (Y-axis) of 30 m, and a chamber direction (Z-axis) of 5 m. The chamber cross-section adopts a horseshoe

ISSN: 2472-3703 DOI: 10.6911/WSRJ.202504_11(4).0005

shape design, and the blast holes are simulated using spherical cavities with a diameter of 20 mm. To accurately simulate the explosive effects, small-sized element meshes are used to divide the blast hole and its surrounding area. The blast holes are located above the arch and on the right side of the side wall, with the specific model configuration shown in Figure 1 and the distribution of monitoring points shown in Figure 2.

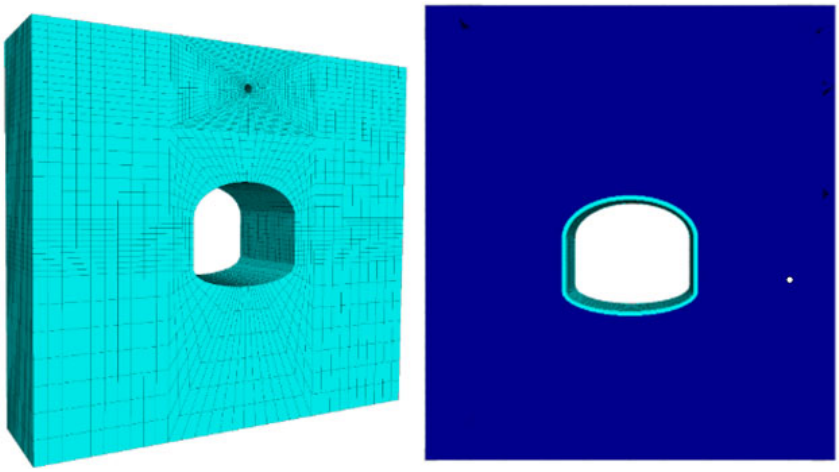

(a)Arch top blast source model diagram (b) Right sidewall blast source model diagram

Figure 1. Computational model for numerical simulation

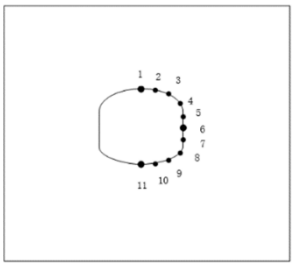

Figure 2. Layout of monitoring points

2.2. Boundary condition setting

The top boundary of the chamber is set as a free boundary to simulate the propagation characteristics of stress waves in a semi-infinite medium. The side and front-back boundaries of the model are subjected to horizontal constraints, while the bottom boundary is subjected to vertical constraints. To prevent stress wave reflections when they reach the model's constrained boundaries, all constrained boundaries are treated with Rayleigh damping viscous boundary conditions. By using static boundary conditions to absorb incident waves, the interference of boundary reflections on the simulation results is further reduced. Additionally, this study employs the local damping mechanism provided by the three-dimensional finite difference software to accurately perform dynamic response analysis. The details are as follows:

$$\tau_n = -\rho C_p V_n, \quad \tau_s = -\rho C_s V_s \tag{4}$$

$$U^{(t+\frac{\Delta t}{2})} = U^{(t-\frac{\Delta t}{2})} + \{\sum F_c^t - (F_s)_c\}\Delta t/m \tag{5}$$

ISSN: 2472-3703 DOI: 10.6911/WSRJ.202504_11(4).0005

$$(F_s)_c = \delta|\sum F_c^t|sgnU^{(t-\frac{\Delta t}{2})} \quad (6)$$

In the formula, V_n and V_s represent the normal and tangential velocity components of the model constraint boundary respectively, m/s; ρ is the material density, kg/m^3; C_p and C_s represent the velocity of P-wave and S-wave respectively, m/s; F_c^t represents the sum of the nodes' force vectors, kN; U represents the node speed, m/s; $(F_s)_c$ represents the joint damping force, kN; Δt represents the calculation time step, s; m represents the node concentration mass, kg; δ represents the damping constant, and δ is 0.8 and 0.16 respectively for static and dynamic calculations.

2.3. Explosion load application

In this paper, the explosive load is directly applied in the form of equivalent stress to the mesh nodes on the inner wall of the blast hole spherical cavity, thereby more accurately simulating the explosion process and its impact on the surrounding rock of the chamber. This method overcomes the limitations of traditional approaches, which cannot fully consider factors such as the charge configuration, explosion parameters, and the location of the blast hole.

The surrounding rock structural material is simulated using solid elements, and its constitutive model is based on the Mohr-Coulomb criterion to more realistically describe the mechanical behavior and failure characteristics of the surrounding rock. The dynamic calculation parameters for the surrounding rock material are shown in Table 1.

Table 1. Dynamic calculation parameters of enclosing rock materials

ρ/kg·m^{-3}	E/GPa	ν	c /MPa	φ/°	σ_t/MPa
1852	2.3	0.46	0.55	47	0.1

The explosion load is calculated as follows:

$$P_b = \frac{1}{8}\rho_0 D_0^2 \left(\frac{R_c}{R_b}\right)^6 \eta \quad (7)$$

Where: ρ_0 is the charge density, kg/m3; D_0 is the explosive detonation speed, m/s; R_c and R_b are the radius of cartridge and hole respectively, m; η is the pressure increase coefficient generated when the explosion product impacts the hole wall.

Convert the velocity time history to the stress time history, and then apply external loads:

$$\sigma_n = 2(\rho C_p)\upsilon_n \quad (8)$$

$$\sigma_s = 2(\rho C_s)\upsilon_s \quad (9)$$

In the formula, σ_n and σ_s respectively represent the normal stress and tangential stress exerted on the boundary element, MPa; ρ is the density; C_p and C_s are the propagation velocities of compression and shear waves in the medium, m/s; v_n and v_s represent the normal and tangential velocity time histories respectively.

The wave velocity of compression and shear waves is determined as follows:

ISSN: 2472-3703 DOI: 10.6911/WSRJ.202504_11(4).0005

$$w = \frac{\sqrt{2C_P}}{3R_b} \tag{10}$$

$$t_R = \frac{\sqrt{2}\ln(n/m)}{2(n-m)w} \tag{11}$$

Where: t_R represents the peak time of the explosion pulse.

3. DYNAMIC RESPONSE CHARACTERISTICS OF SURROUNDING ROCK OF DEEP UNDERGROUND CAVERN

In the operation of deep underground engineering, the deformation of the surrounding rock directly reflects the extent of disturbance to the rock mass caused by explosive loads. This paper primarily analyzes the deformation of the surrounding rock around the tunnel under external impact loads, aiming to explore the deformation laws of the surrounding rock.

3.1. Displacement analysis of surrounding rock

(1) Displacement analysis of surrounding rock of deep underground cavern under the action of top blasting

The displacement cloud map of the surrounding rock at the tunnel section under top blast is shown in Figure 3-4. The influence range of the explosion extends outward in a "U" shape, and as time progresses, the affected area gradually increases and ultimately stabilizes. The displacement of the medium elements directly above the blast hole is particularly significant, with the maximum displacement reaching up to 48 cm. As seen in Figure 4, in the X-direction, the displacement of the elements above the blast hole exhibits a "U" shape, gradually expanding outward; when the time reaches 100 ms, the displacement distribution stabilizes and the shape evolves into an "X."

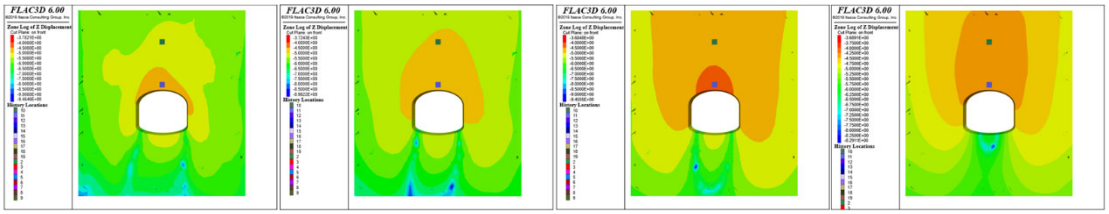

(a) t=3 ms (b) t=10 ms (c) t=20 ms (d) t=100 ms

Figure 3. Vertical displacement map of top blast chamber

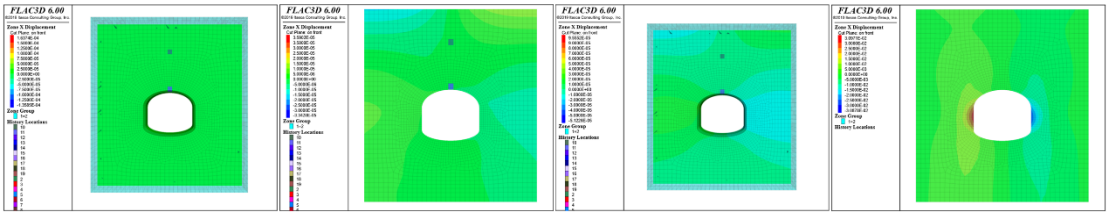

(a) t=3 ms (b) t=10 ms (c) t=20 ms (d) t=100 ms

Figure 4. Horizontal displacement map of top blast chamber

As shown in Figure 5, during the early stages of the explosion, a slight deformation of about 17 cm occurs at the section; as the explosion progresses, the surrounding rock load is gradually released, and the displacements at the crown and the invert begin to increase. During the early

ISSN: 2472-3703 DOI: 10.6911/WSRJ.202504_11(4).0005

explosion stage, the displacement at the crown and invert increases approximately linearly. The crown displacement rapidly increases from 17 cm to 40 cm, and the invert displacement increases from 20 cm to over 50 cm. After the peak load is reached, the vertical deformation of the tunnel is controlled, and the deformation rate gradually slows down, with the displacement curves for the crown and invert tending to stabilize.

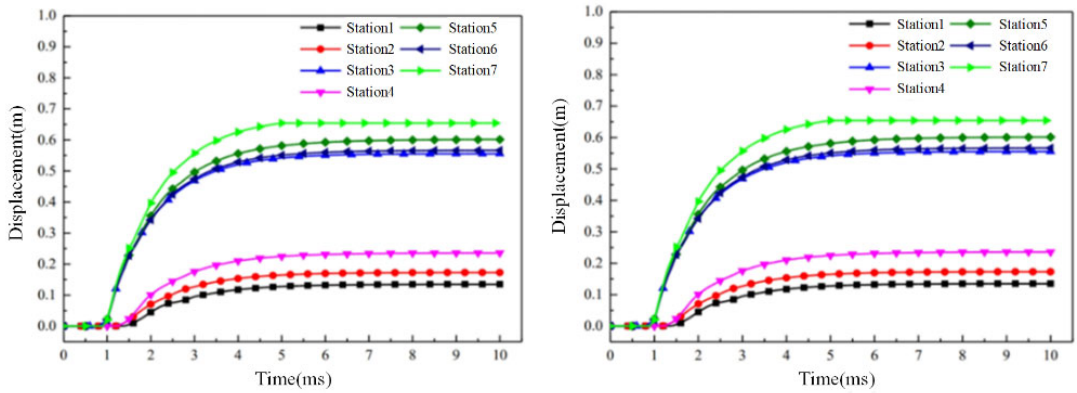

(a)Vertical displacement (b) horizontal displacement

Figure 5. Displacement time curve of the measuring point of the roof explosion chamber

(2) Displacement analysis of surrounding rock of deep underground cavern under lateral explosion

From Figures 6-8, it can be seen that the vertical displacement of the tunnel shows an "O" shape at the beginning of the explosion, gradually spreading to both sides over time. In terms of horizontal displacement, the tunnel displacement near the blast hole gradually evolves from an "O" shape to a "W" shape, and the affected area stabilizes around 100 ms. The displacement distribution in the tunnel is influenced by the reflection and diffraction of stress waves, especially the displacement on the blast face of the underground tunnel, which is significantly larger than that on the non-blast face. Since the explosion source is located on the right side of the tunnel, the displacement of the left wall and the invert is significantly lower than that of the crown and the right wall.

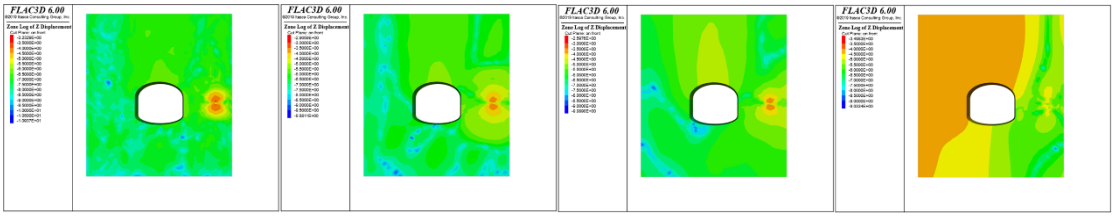

(a) t=3 ms (b) t=10 ms (c) t=20 ms (d) t=100 ms

Figure 6. Vertical displacement map of side blast chamber

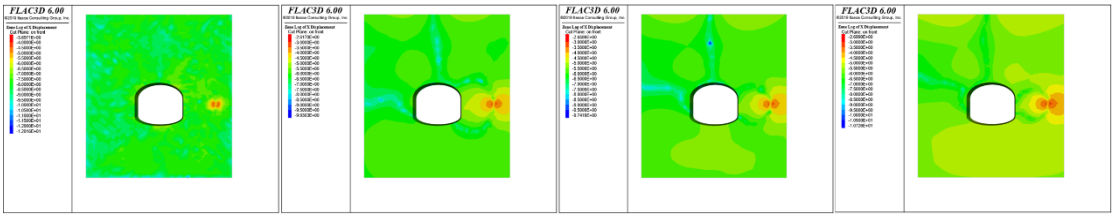

(a) t=3 ms (b) t=10 ms (c) t=20 ms (d) t=100 ms

Figure 7. Horizontal displacement map of side blast chamber

ISSN: 2472-3703 DOI: 10.6911/WSRJ.202504_11(4).0005

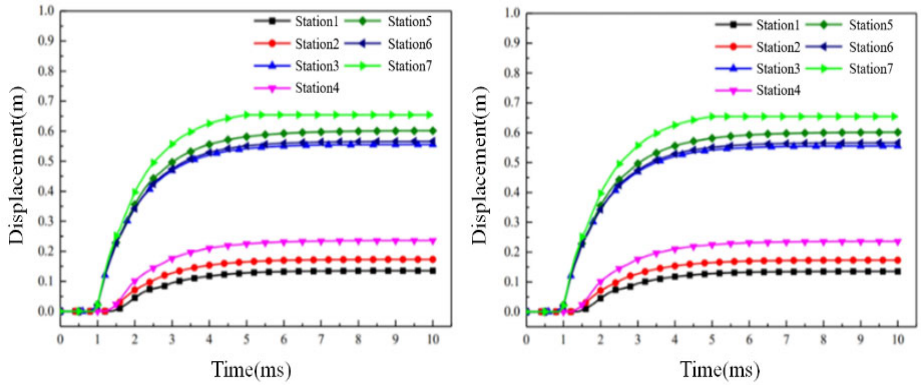

(a)Vertical displacement (b) horizontal displacement

Figure 8. Displacement time curve of the measurement point of the side explosion chamber

Whether the explosion method is top-blast or side-blast, the deformation characteristics of the tunnel consistently show crown settlement and invert heaving. The deformation near the blast hole is the most significant, and numerous cracks appear in the rock mass, becoming potential collapse zones. The range and extent of the explosion's effect are closely related to the peak pressure of the explosives.

3.2. Stress analysis of surrounding rock

(1) Stress analysis of surrounding rock of deep underground cavern under the action of top burst

Figure 9 shows the vertical stress distribution of the surrounding rock under the effect of top-blast, where positive values indicate tensile stress and negative values indicate compressive stress. Under the explosive load, the compressive stress around the blast hole gradually increases and spreads outward. During the stress wave growth stage, tensile stress zones appear at the top and bottom of the tunnel, eventually forming a through-tensile region extending to both sides of the model. At the same time, a noticeable compressive stress zone appears at the tunnel's arch foot, indicating that the medium elements in this region have reached the failure stage. As the explosion progresses, the stress wave enters the attenuation stage, and the tensile stress zones gradually stabilize. When the stress wave peaks and begins to decay, cracks rapidly develop in the crown, invert, arch waist, and sidewalls.

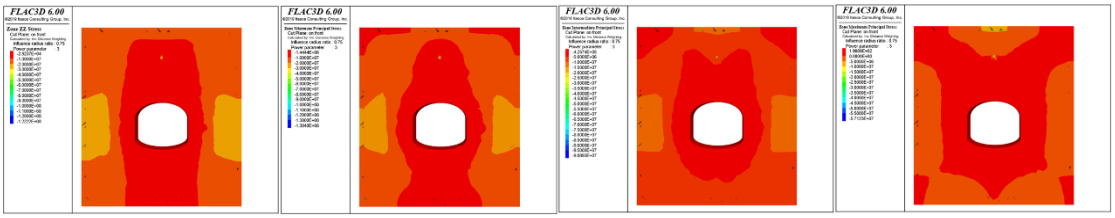

(a) t=3 ms (b) t=10 ms (c) t=20 ms (d) t=100 ms

Figure 9. Vertical stress distribution of the roof explosion chamber

Figure 10 shows the horizontal stress distribution of the surrounding rock under top-blast. Under the explosive load, the surrounding rock of the tunnel moves toward the free surface, leading to uneven deformation of the tunnel, which in turn causes a redistribution of the stress field. This change results in uneven stress concentration on the tunnel surface, forming potential fracture zones. Particularly near the crown, significant changes occur in the maximum principal stress field of the surrounding rock. Within a range of 5-6 meters near the crown, the

ISSN: 2472-3703 DOI: 10.6911/WSRJ.202504_11(4).0005

stress change is relatively evident, while the impact range near the sidewalls is relatively small, confined to 2-3 meters.

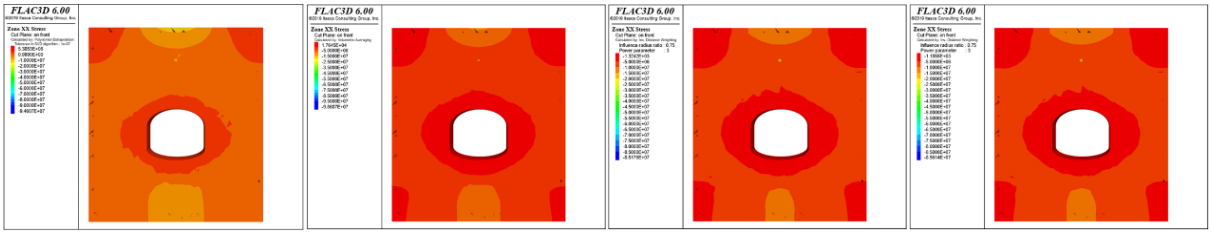

(a) t=3 ms (b) t=10 ms (c) t=20 ms (d) t=100 ms

Figure 10. Horizontal Stress Distribution in Top Blast Chamber

Figure 11 presents the stress-time curve for the surrounding rock of the tunnel. From the figure, it can be seen that the maximum principal stress of the surrounding rock primarily alternates between stress concentration zones and regions where stress is reduced near open faces, especially at the center of the crown, the center of the invert, and the sidewalls, where this phenomenon is particularly noticeable. The maximum principal stress on the surface of the tunnel surrounding rock is concentrated between 6-7 MPa, primarily at the intersections of the sidewalls, crown, and invert. As the explosive load increases, the degree of stress concentration gradually intensifies. When the explosive load peaks, the potential damage to the underground tunnel gradually increases, and the maximum principal stress shifts from tensile stress to compressive stress. After the peak explosive load, as the load gradually decreases, the maximum principal stress at the arch shoulders and arch foot becomes significantly higher than at the crown and invert. This is mainly because these regions are not only affected by the explosive load but also by the compressive deformation of the overlying rock, leading to more pronounced stress concentration.

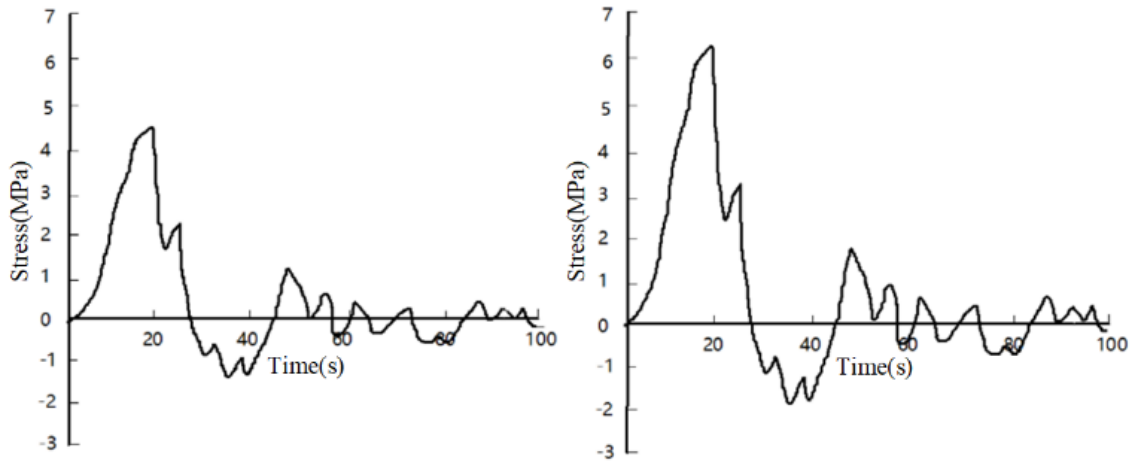

(a) vertical stress (b) horizontal stress

Figure 11. Horizontal Stress Curve of Top Blast Chamber

(2) Stress analysis of surrounding rock of deep underground cavern under lateral explosion

Figure 12 shows the vertical stress distribution of the tunnel surrounding rock. Under the explosive load, the stress state of the surrounding rock undergoes significant changes, with the compressive stress zone expanding outward from the center of the blast hole. During the stress wave growth phase, tensile stress zones appear below the right arch and invert, which gradually

ISSN: 2472-3703 DOI: 10.6911/WSRJ.202504_11(4).0005

expand and eventually form a through zone, becoming potential fracture zones. At the same time, at the right arch of the tunnel, a clear compressive stress zone appears, indicating that the medium elements in this region have reached the failure stage.

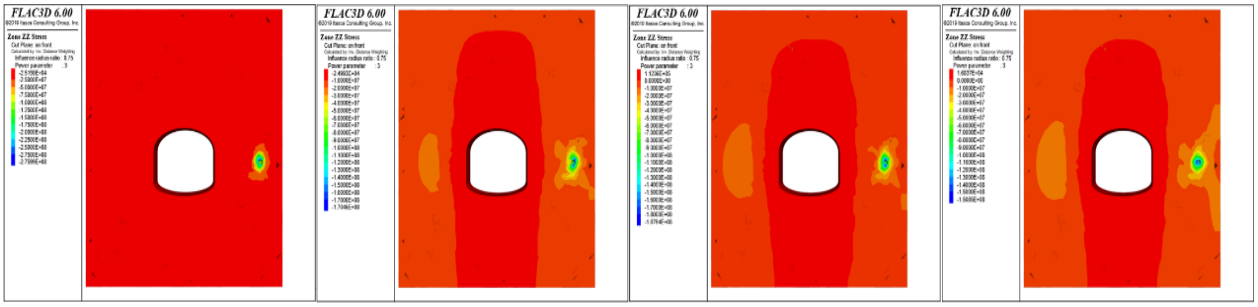

(a) t=3 ms (b) t=10 ms (c) t=20 ms (d) t=100 ms

Figure 12. Vertical stress distribution of side blast chamber

As the explosion time progresses, the stress wave enters the attenuation phase, and the tensile stress zones in the model gradually stabilize, with the stress values remaining constant. Figure 13 shows the horizontal stress distribution in the tunnel, which is similar to the vertical stress distribution.

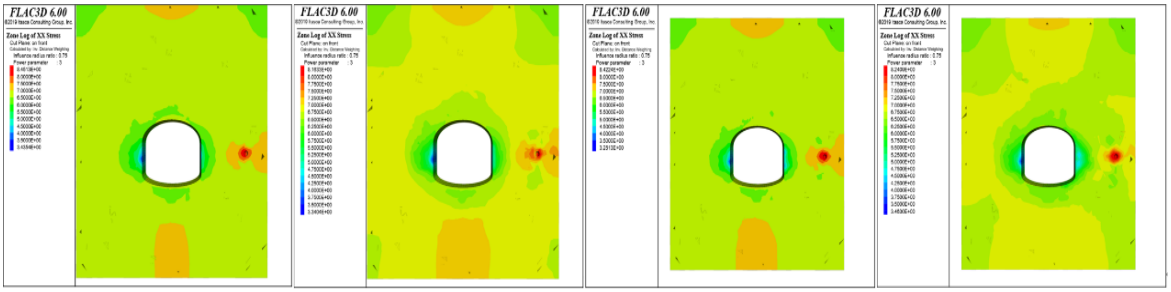

(a) t=3 ms (b) t=10 ms (c) t=20 ms (d) t=100 ms

Figure 13. Horizontal stress distribution of side blast chamber

Figure 14 shows the stress-time curve under side-blast. During the explosion process, the explosive load undergoes alternating tensile and compressive stresses, and the stress gradually decays and stabilizes. This indicates that the simulated results of the explosive stress wave are consistent with the actual situation, and the simulation method, mesh division, and boundary conditions are reasonably set. The pressure wave signals at each measurement point exhibit exponential decay as the distance from the explosion center increases, indicating that the propagation of the stress wave is closely related to the damping characteristics of the rock mass. The selection of material parameters has a significant impact on the calculation results. It is worth noting that when the explosion wave diffracts around the underground tunnel, the peak load on the surrounding rock of the tunnel is always compressive, and it gradually decreases from the crown to the tunnel bottom. This is due to the large contact area of the arch structure, and the diffraction effect of the explosion wave causes a time delay between the peak load on the crown and sidewalls and the peak load at the bottom.

ISSN: 2472-3703 DOI: 10.6911/WSRJ.202504_11(4).0005

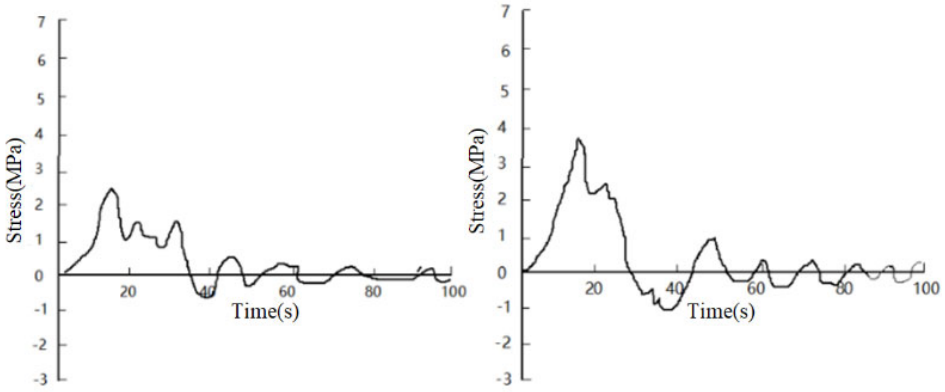

(a)vertical stress **(b) horizontal stress**

Figure 14. Horizontal stress time curve of side blast chamber

3.3. Velocity and acceleration analysis of surrounding rock

(1) Velocity and acceleration analysis of surrounding rock in deep underground cavern under the action of top burst

The velocity vector contour map under the explosion load is shown in Figure 15, and the acceleration vector contour map is shown in Figure 16. The monitoring data indicates that the velocity at all measurement points initially decreases to a minimum, then gradually increases and finally stabilizes, with oscillations appearing near the zero horizontal line. At t = 3 ms, the velocity peak on both sides of the chamber gradually increases, which is mainly due to the presence of the chamber's free surface, which amplifies the velocity changes. The reflection and propagation characteristics of the free surface lead to a significant increase in velocity in localized areas. At t = 10 ms, the rate of velocity increase begins to slow down, and the particles near the upper and lower surfaces resume a more consistent velocity movement trend, indicating that as the explosive load decays, the dynamic response inside the chamber gradually stabilizes.

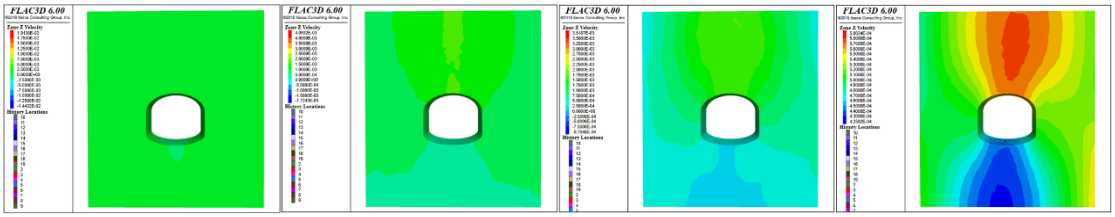

(a) t=3 ms (b) t=10 ms (c) t=20 ms (d) t=100 ms

Figure 15. Vector cloud of velocity in the headblast chamber

At t = 20 ms, the peak of the stress wave in the explosion near field rapidly decreases. When the stress level drops below the compressive strength of the rock, the chamber's compressive damage tends to stop, and the peak velocity of the particles begins to stabilize. At this point, the main effect of the explosive load has decayed, and the stress state of the rock mass stabilizes. However, when the stress wave reaches the chamber surface, the particle velocity peaks further amplify. This is due to the explosive load creating a new stress field on the chamber surface, leading to a concentration of stress within the underground chamber. The surface region is strongly influenced by the explosion wave, causing a further increase in local stress and velocity.

ISSN: 2472-3703 DOI: 10.6911/WSRJ.202504_11(4).0005

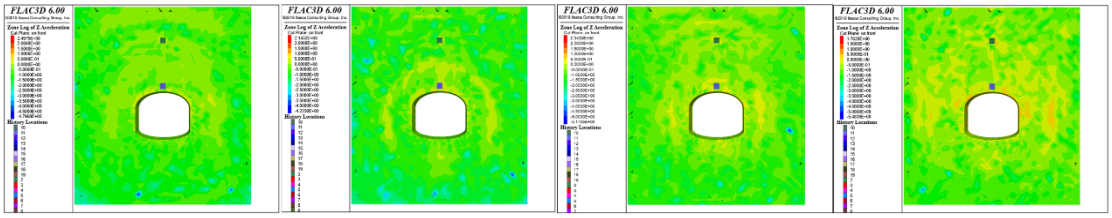

(a) t=3 ms (b) t=10 ms (c) t=20 ms (d) t=100 ms

Figure 16. Vector diagram of acceleration in the head blast chamber

Figure 17 shows the time history curves of the top explosion chamber measurement points. In the initial stage, the velocity at all measurement points increases rapidly, reaching the peak velocity around 10 ms, then undergoing multiple decrease-increase cycles, stabilizing around 80 ms. After the peak load is reached, the acceleration at all measurement points shows a decreasing trend, reaching the minimum value at 14 ms, followed by multiple increase-decrease cycles, and stabilizing around 80 ms.

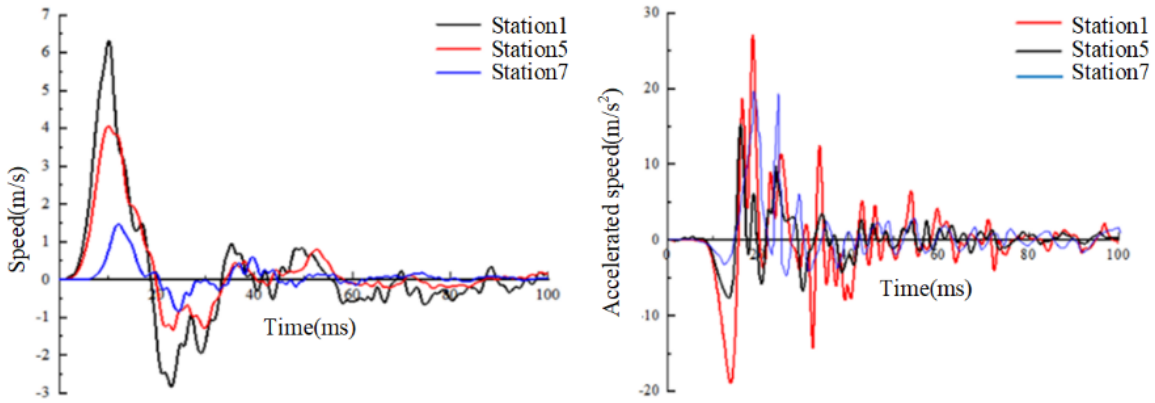

(a) Velocity time history curve (b) Acceleration time history curve

Figure 17. Time course curve of the measuring point of the roof explosion chamber

(2) Velocity and acceleration analysis of surrounding rock of deep underground cavern under lateral explosion

The velocity vector contour map under lateral explosion load is shown in Figure 18, and the acceleration vector map is shown in Figure 19. At t = 7 ms, the velocity peak on both sides of the chamber gradually increases, and the chamber's free surface amplifies both velocity and acceleration. At t = 10 ms, the rate of velocity increase slows, and the particles near the upper and lower surfaces return to a similar velocity movement. At t = 20 ms, the velocity increase starts to stabilize. At t = 100 ms, no significant changes in particle velocity occur.

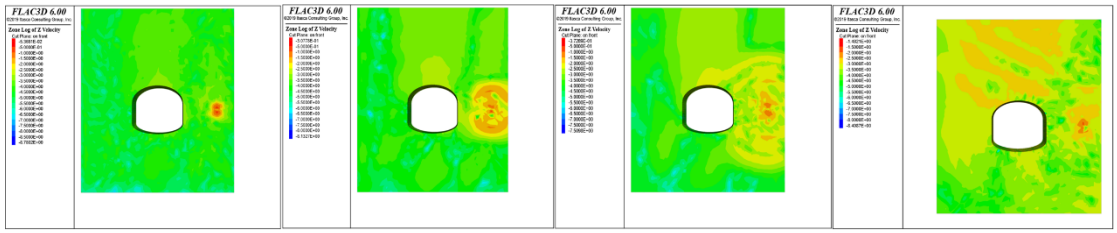

(a) t=7 ms (b) t=10 ms (c) t=20 ms (d) t=100 ms

Figure 18. Velocity vector cloud of side blast chamber

ISSN: 2472-3703 DOI: 10.6911/WSRJ.202504_11(4).0005

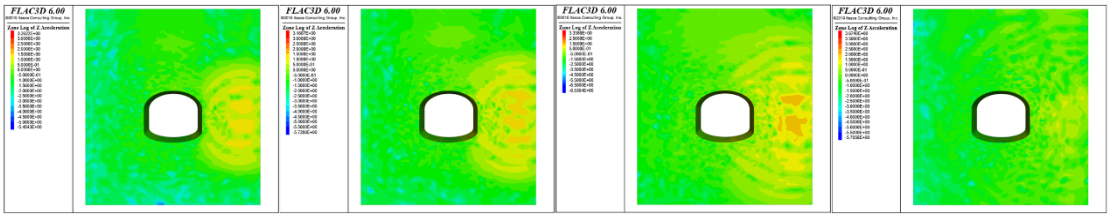

(a) t=3 ms (b) t=10 ms (c) t=20 ms (d) t=100 ms

Figure 19. Vector diagram of acceleration in side blast chamber

The peak of the stress wave in the explosion near field decreases rapidly. When the stress drops below the compressive strength of the rock, the chamber is no longer significantly compressed, and the acceleration remains stable. When the stress wave propagates to the chamber surface, the particle velocity peaks again amplify. This is due to the formation of a new stress field on the chamber surface, leading to stress concentration inside the underground chamber. When the explosion wave propagates to the floor slab, the floor slab moves downward under the influence of the surrounding walls, but the displacement is small. Since the void space is above the floor slab, the acceleration of the floor slab points inward toward the chamber, causing it to move upward. The entire floor slab undergoes up-and-down repetitive motion, with the upward motion lasting longer than the downward motion. Therefore, the peak acceleration of the chamber floor slab is significantly lower than that of the arch roof.

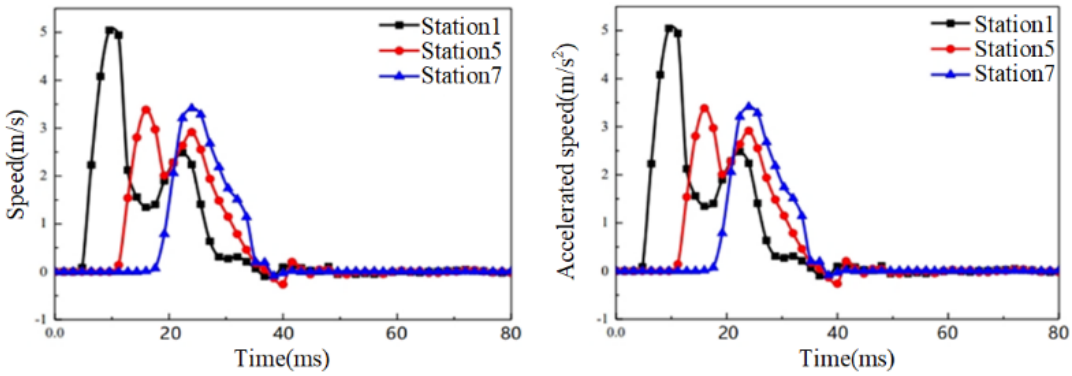

(a) Velocity time history curve (b) Acceleration time history curve

Figure 20. Side-blast chamber measurement point time curve

Figure 20 shows the time history curves of the side explosion chamber measurement points. In the initial stage, the velocity at all measurement points increases rapidly, reaching the peak velocity around 10 ms, then undergoing multiple decrease-increase cycles, stabilizing around 40 ms. After the peak load is reached, the acceleration at all measurement points increases, reaching the maximum value at 11 ms, followed by multiple decrease-increase cycles, stabilizing around 40 ms.

3.4. Strain analysis of surrounding rock

(1) Strain analysis of surrounding rock of deep underground cavern under the action of top burst

The circumferential strain of the chamber is an important indicator for evaluating the chamber's anti-blast capability. Taking the top explosion of the chamber in Figure 21 as an example, by observing the circumferential strain peaks at various measurement points, it can

ISSN: 2472-3703 DOI: 10.6911/WSRJ.202504_11(4).0005

be seen that the explosion causes the chamber's arch roof to move downward and undergo lateral tensile deformation, leading to tensile strain from the arch roof to the waist area.

Since the tensile strength of the rock mass is much lower than its compressive strength, and important instruments are usually installed at the arch bottom, explosions at the arch roof and sidewalls must be avoided. When the explosion occurs above the chamber, the arch foot and floor mainly bear compressive strain, causing the arch to descend and triggering lateral compression in the waist. Detailed measurements show that when the shock wave reaches the monitoring point, the circumferential strain curve fluctuates and then stabilizes. The strain response of the rock mass is not smooth, but involves complex transitions between tensile and compressive strains. As the observation point moves closer to the arch roof, the compressive strain gradually decreases, while the tensile strain increases accordingly.

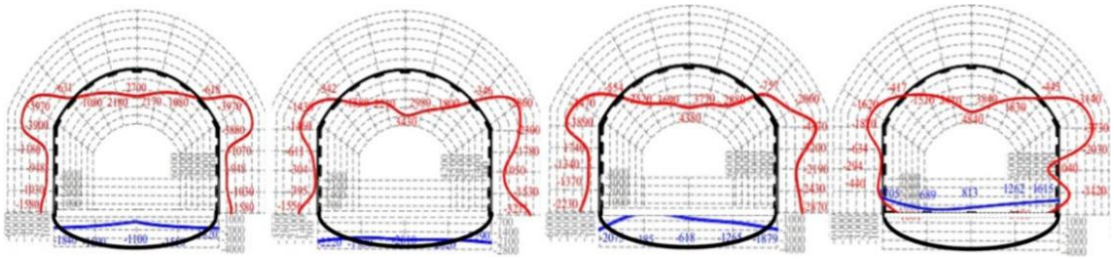

(a) t=3 ms (b) t=10 ms (c) t=20 ms (d) t=100 ms

Figure 21. Strain distribution in the head-blasted chamber

(2) Strain analysis of surrounding rock of deep underground cavern under lateral explosion

When an explosion source is present on the right side of the arch wall, the stress wave generated by the explosion propagates horizontally to the chamber, causing the sidewall to undergo tensile strain, directly affecting the sidewall rock mass, leading it to move inward toward the chamber, thereby inducing vertical tensile strain in the rock mass. This indicates that in the case of lateral explosion, the chamber floor slab is subjected to pressure from both side arch walls, causing the floor slab to rise upward and undergo lateral tensile deformation, resulting in tensile strain. As the surrounding rock near the waist and arch foot is supported by the rock below, it reduces the likelihood of tensile strain.

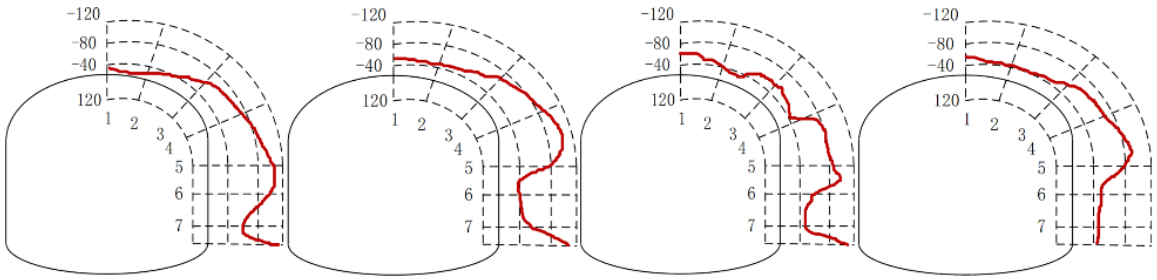

(a) t=3 ms (b) t=10 ms (c) t=20 ms (d) t=100 ms

Figure 22. Strain distribution of side blast chamber

Comparative analysis shows that the circumferential strain peak values decrease from the arch roof to the arch foot and then increase. The lack of effective support at the arch roof causes the surrounding rock strain in this area to increase, while the arch foot, as the connecting point, is prone to stress concentration and bears greater stress, leading to increased strain. The arch foot mainly experiences compressive strain, while the arch roof undergoes tensile strain. Since the surrounding rock's ability to withstand pressure is stronger than that of tensile force, the

ISSN: 2472-3703 DOI: 10.6911/WSRJ.202504_11(4).0005

arch roof is more susceptible to damage under explosion impact. If there is a lateral explosion source, tensile strain will occur at the lower-right corner of the arch wall, while the rock mass on the non-facing explosion side of the chamber mainly experiences compressive strain.

3.5. Plastic zone analysis of surrounding rock

(1) Analysis of plastic zone of surrounding rock of deep underground cavern under the action of top blasting

Figure 23 shows the distribution of the plastic zone in the chamber under the action of the stress wave. The analysis results indicate that due to the high peak explosive pressure, cracks may form in the chamber's arch roof area. Over time, the plastic zone gradually stabilizes, with the media units near the blast hole mainly exhibiting tensile shear failure, while those farther from the blast hole predominantly showing tensile failure.

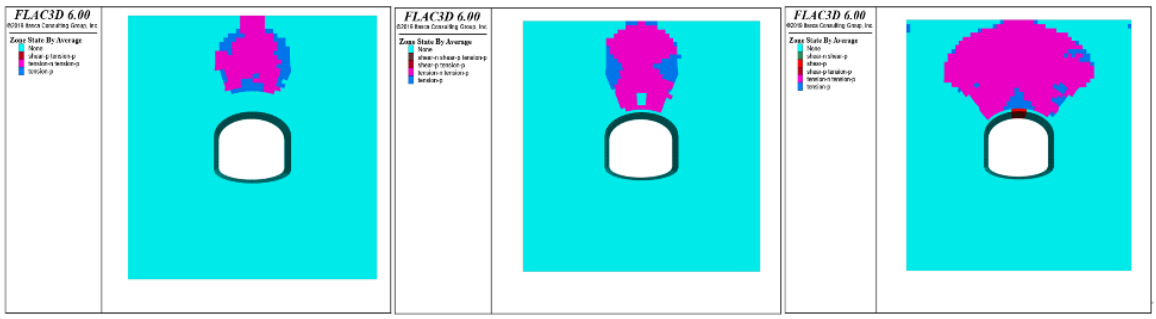

(a) t=3 ms (b) t=10 ms (c)t=20 ms

Figure 23. Plastic zone cloud map of the roof explosion chamber

(2) Analysis of plastic zone of surrounding rock of deep underground cavern under lateral explosion

Figure 24 shows the plastic zone distribution map under the action of the stress wave. When the dynamic response time of the underground chamber under explosive load reaches 100 ms, the plastic zone stabilizes. The media units near the blast point mainly exhibit tensile shear failure, while those farther from the blast point mainly exhibit tensile failure. Due to the high peak explosive pressure, cracks may appear in the chamber's sidewall.

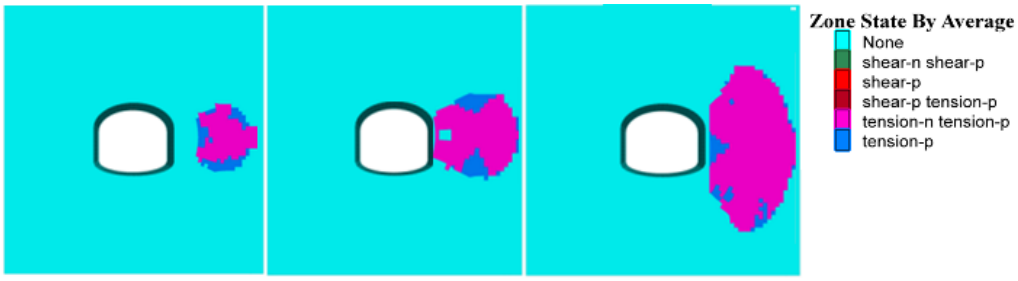

(a) t=3 ms (b) t=10 ms (c) t=20 ms

Figure 24. Plastic zone cloud map of side blast chamber

Whether it's a top or side explosion, under the action of the explosion stress wave, the chamber model exhibits both shear and tensile plastic states. Before the stress wave reaches the chamber, the contact media first undergoes tensile yielding. As the stress wave propagates and the chamber attenuates it, the expansion of the tensile plastic zone slows down significantly. During the loading process, the plastic failure zone develops rapidly. The degree of damage caused by different loading speeds tends to be consistent, indicating that the loading speed has

ISSN: 2472-3703 DOI: 10.6911/WSRJ.202504_11(4).0005

a limited effect on the final damage. However, there is a clear relationship between the development speed of the damage zone and the loading speed; the faster the loading speed, the faster the expansion of the damage zone.

4. DYNAMIC RESPONSE CHARACTERISTICS OF SURROUNDING ROCK OF ANCHORING CAVITY

Figure 25 shows the model diagram of the anchored chamber. The net distance between the upper arch roof and the lower arch floor is 5.3 m, and the net distance between the left and right sidewalls is 6 m. The boundary of the model is set to 4 times the tunnel diameter, with a burial depth of 600 m. The overall dimensions of the model are 5 m in width, 5 m in height, and 3 m in depth. The mechanical boundary conditions of the model are: a pressure of 30 MPa applied at the top, normal constraints on the left, right, front, and rear, and fixed at the bottom.

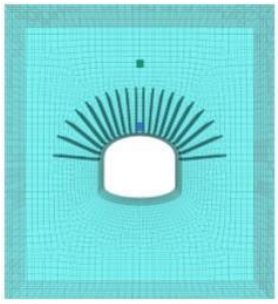

Figure 25. Model drawing of the anchoring chamber

By comparing the dynamic responses of the anchored and unanchored chambers under explosive load, this study verifies the effectiveness of anchoring technology in enhancing the underground chamber's anti-blast performance (Figures 26-27, Tables 2-3). By analyzing displacement deformation, maximum peak displacement, and particle velocity data, the following conclusions can be drawn: the anchored chamber shows significant advantages in improving chamber deformation and stress, reducing by 29.7% and 27.6%, respectively; however, the anchored chamber has less pronounced effects on improving measurement point velocity and acceleration, reducing by 2.91% and 2.44%, respectively. This indicates that the anchor support technology effectively enhances the overall stability of the surrounding rock by adjusting the dynamic response and vibration modes of the surrounding rock particles, although the impact on velocity and acceleration is small, the significant reduction in displacement and stress still effectively improves the anti-blast performance of the chamber.

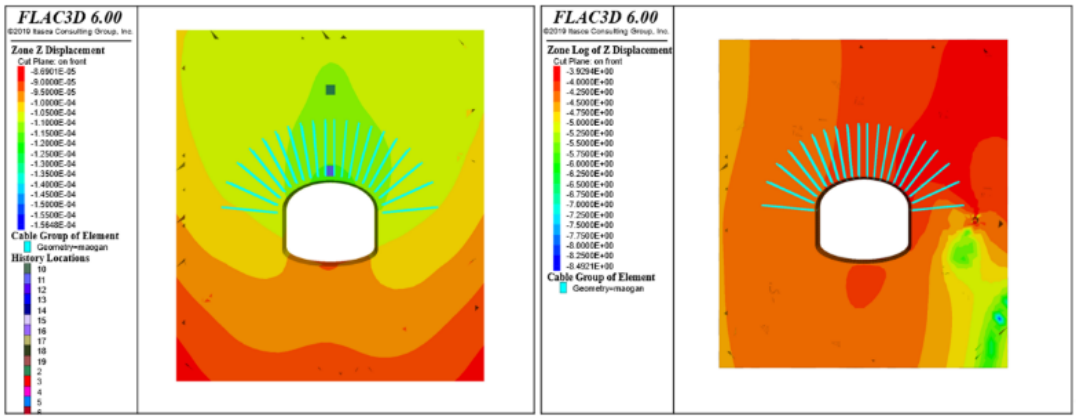

(a) Top blast chamber (b) Side blast chamber

Figure 26. Vertical displacement cloud of anchored cavities

ISSN: 2472-3703 DOI: 10.6911/WSRJ.202504_11(4).0005

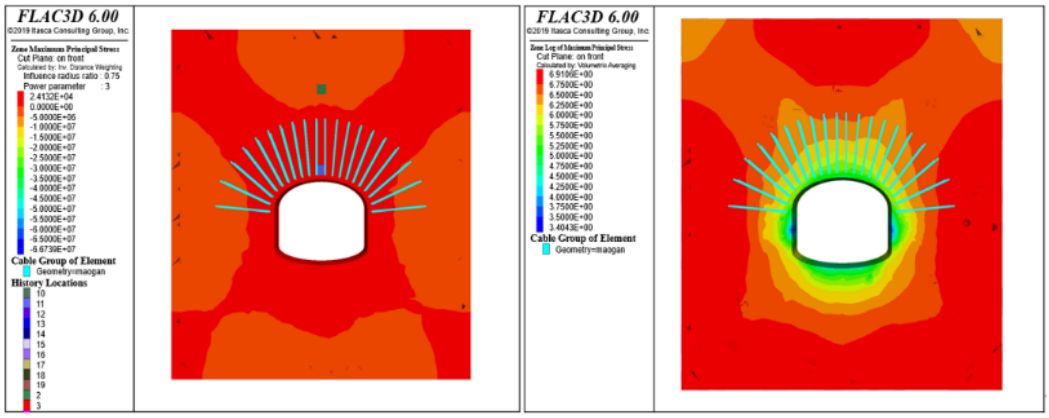

(a) Top blast chamber (b) Side blast chamber

Figure 27. Vertical stress cloud for anchored cavities

Table 2. Displacement and Stress Changes at Cavity Measurement Points

measure point	Anchorage condition	displacement(cm)	distinction(%)	stress(MPa)	distinction(%)
1	unanchored	8.21	-23.9	8.73	-27.3
	anchoring	6.13		7.55	
2	unanchored	7.84	-28.9	8.35	-25.9
	anchoring	5.61		7.19	
3	unanchored	5.76	-34.7	6.68	-32.7
	anchoring	3.58		5.55	
4	unanchored	7.59	-30.5	8.08	-27.5
	anchoring	5.21		6.76	
5	unanchored	4.41	-31.8	6.32	-29.8
	anchoring	2.98		5.24	
6	unanchored	4.32	-29.4	6.86	-26.7
	anchoring	3.12		5.69	
7	unanchored	4.17	-28.7	6.75	-23.7
	anchoring	3.02		5.63	
average			-29.7		-27.6

Table 3. Velocity and acceleration variations at cave measurement points

measure point	Anchorage condition	accelerated speed(m/s^2)	distinction(%)	speed(m/s)	distinction(%)
1	unanchored	6.24	-2.5	6.78	-2.7
	anchoring	6.13		6.51	
2	unanchored	5.71	-2.9	6.35	-3.0
	anchoring	5.51		6.14	
3	unanchored	4.02	-2.7	4.68	-2.6
	anchoring	3.78		4.55	
4	unanchored	5.39	-3.1	6.08	-2.8
	anchoring	5.21		5.76	
5	unanchored	3.21	-3.4	4.32	-2.2
	anchoring	2.98		4.24	
6	unanchored	3.35	-2.1	3.86	-1.7
	anchoring	3.12		3.69	
7	unanchored	3.28	-3.7	3.75	-2.1
	anchoring	3.02		3.63	
average			-2.91		-2.44

ISSN: 2472-3703 DOI: 10.6911/WSRJ.202504_11(4).0005

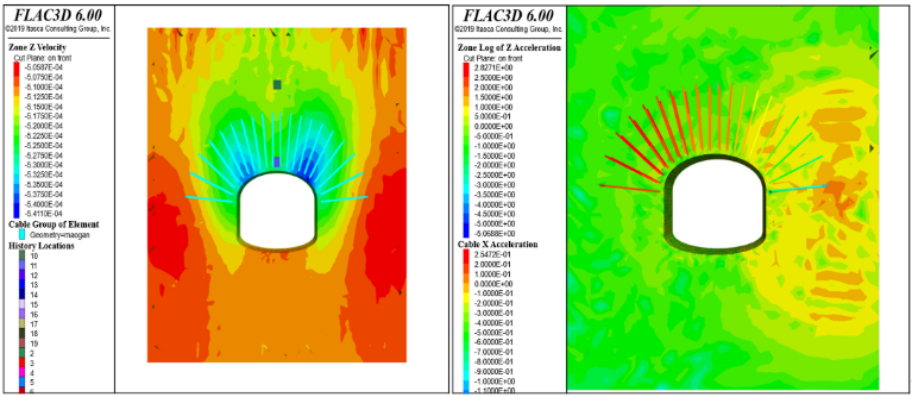

(a)Top blast chamber **(b) side blast chamber**

Figure 28. Velocity cloud of anchored cavities

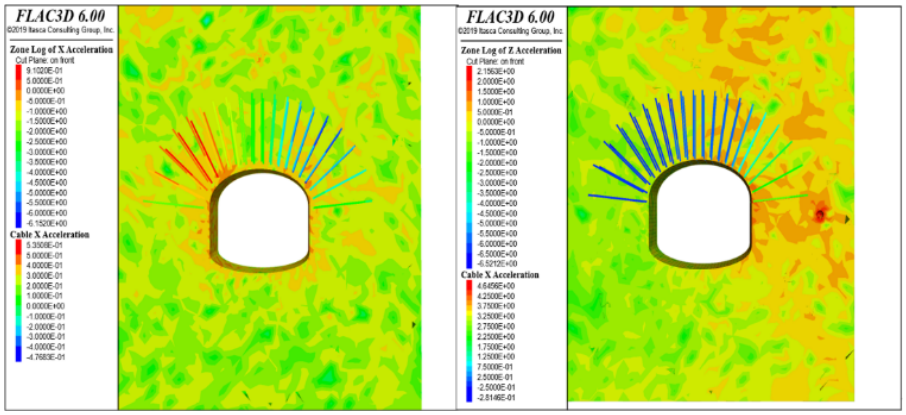

(a)Top blast chamber **(b) side blast chamber**

Figure 29. Acceleration cloud for anchored cavities

5. CONCLUSION

This paper uses a three-dimensional finite difference software for numerical simulation to deeply explore the dynamic characteristics of displacement, velocity, stress, and plastic deformation of the cavern under different explosion pressure conditions. The main conclusions are as follows:

(1) As the peak explosion pressure increases, the peak velocity shows a significant upward trend. The vertical displacement of the surrounding rock of the cavern primarily manifests as roof settlement and floor uplift. As the instantaneous impact load increases, both the roof settlement displacement and the floor uplift displacement gradually increase. Under the action of explosive load, the underground structure, particularly the bottom support area of the cavern, exhibits a high sensitivity to failure. This result suggests that special attention should be paid to these sensitive areas during the design phase, with reinforcement measures taken to improve the blast resistance and stability of the structure.

(2) Under the explosive load, the surrounding rock of the cavern shows obvious compressive and tensile damage. In the initial stage, the compressive stress near the borehole increases rapidly and extends outward to the surrounding cavern. By 7 ms, tensile stress concentration first appears at the roof and floor areas of the cavern. As time progresses, these tensile stresses gradually increase and spread outward, reaching a stable state at 100 ms. As the explosion load intensity increases, the tensile stress region at the top and floor of the cavern gradually expands. In addition, the variation trends of the maximum and minimum principal stresses near the

ISSN: 2472-3703 DOI: 10.6911/WSRJ.202504_11(4).0005

borehole are similar. In the initial stage, tensile stress appears at the top and floor of the cavern, and these tensile stress regions gradually expand and stabilize. By 100 ms, a tensile stress region forms on one side of the cavern, while a compressive stress region forms on the other side.

(3) The cavern exhibits a dual plastic state under the action of the explosive stress wave: tensile and shear. Before the stress wave reaches the cavern, the surrounding medium has already entered the tensile yield state. When the stress wave arrives, the lining structure of the cavern exhibits a tensile plastic state. However, due to the further propagation of the stress wave and the attenuation effect of the cavern on the stress wave, the expansion of the tensile plastic region gradually slows down. By 100 ms, the plastic region around the cavern gradually develops and stabilizes. During this process, the medium units near the borehole mainly experience tensile shear failure, while regions farther from the borehole primarily exhibit tensile failure. As the peak explosion pressure increases, the area of the plastic region around the cavern also increases correspondingly.

REFERENCES

[1] Wang Guangyong, Wang Taotao, Pei Chenhao, et al. Distribution of vibration velocity and influence of bolt parameters of caverns reinforced by rock bolts under blast loads, Chinese Journal of Applied Mechanics, vol. 37 (2020), No.5, p.2207-2213+2334.

[2] Xu J H, Kang Y, Wang X C, et al. Dynamic characteristics and safety criterion of deep rock mine opening under blast loading, International Journal of Rock Mechanics and Mining Sciences, vol. 119 (2019), p.156-167.

[3] Wu C, Hao H. Numerical prediction of rock mass damage due to accidental explosions in an underground ammunition storage chamber, Shock Waves, vol. 15 (2006), No.1, p.43-54.

[4] Wang Guangyong, Wang Chao, Yu Yongqiang, et al. Research on Anchored Effect of Tunnels under Explosion Load in Different Directions, Chinese Journal of Underground Space and Engineering, vol. 13 (2017), No.6, p.1645-1653.

[5] XU Gancheng, YUAN Weize, GU Jincai, et al. Explosive resistivity of anchored cavern surface rock, Chinese Journal of Rock Mechanics and Engineering, vol. 34 (2015), No.9, p.1767-1776.

[6] CHEN Anmin, GU Jincai, XU Jingmao, et al. Model test study of tunnel mechanical characteristics under plane charge explosion, Rock and Soil Mechanics, vol. 32 (2011), No.9, p.2603-2608.

[7] Deng X F, Zhu J B, Chen S G, et al. Numerical study on tunnel damage subject to blast-induced shock wave in jointed rock masses, Tunnelling and Underground Space Technology, vol. 43 (2014), No.6, p.88-100.

[8] GU Jincai, CHEN Anmin, XU Jingmao, et al. Model test study of failure patterns of anchored tunnel subjected to explosion load, Chinese Journal of Rock Mechanics and Engineering, vol. 8 (2008), No.7, p.1315-1320.

[9] WANG Guangyong, GU Jincai, CHEN Anmin, et al. Model test research on anti-explosion capacity of underground openings with end wave-decay by holes and reinforced by dense rock bolts, Chinese Journal of Rock Mechanics and Engineering, vol. 29 (2010), No.1, p.51-58.

[10] XU Jingmao, GU Jincai, CHEN Anmin, et al. Model test study of anti-explosion capacity of anchored tunnel with local lengthening anchors in arch springing, Chinese Journal of Rock Mechanics and Engineering, vol. 31 (2012), No.11, p.2182-2186.

[11] Chang X, Wang G Y, Tang C N, Ru Z L. Dynamic behavior of cement-mortar cavern reinforced by bars, Engineering Failure Analysis, vol. 55 (2015), p.343-354.

ISSN: 2472-3703 DOI: 10.6911/WSRJ.202504_11(4).0005

[12] Saikat K, Vedala R S. A numerical modelling approach to assess the behaviour of underground cavern subjected to blast loads, International Journal of Mining Science and Technology, vol. 28 (2018), No.6, p.975-983.

[13] Mitelman A, Elmo D. Analysis of tunnel support design to withstand spalling induced by blasting, Tunnelling & Underground Space Technology Incorporating Trenchless Technology Research, vol. 51 (2016), p.354-361.

[14] Koneshwaran S, Thambiratnam D P, Gallage C. Blast Response and Failure Analysis of a Segmented Buried Tunnel, Structural Engineering International, vol. 25 (2015), No.4, p.419-431.

[15] Mobaraki B, Vaghefi M. Numerical study of the depth and cross-sectional shape of tunnel under surface explosion, Tunnelling & Underground Space Technology Incorporating Trenchless Technology Research, vol. 47 (2015), p.114-122.